• Basic Research •

Alkali burn injury model of meibomian gland dysfunction in mice

Yong Li[1,2], Ya-Qiong Yang[1,3], Yong Lin[4], Ke Yan[5], Yu-Fei Lyu[4], Zhao-Qiang Zhang[1,3], Cai-Hong Huang[1,3], Jiao-Yue Hu[1,3], Zu-Guo Liu[1,2,3,4]

[1]Xiamen University Affiliated Xiamen Eye Center, Eye Institute of Xiamen University, School of Medicine, Xiamen University, Xiamen 3611002, Fujian Province, China
[2]The Second Affiliated Hospital, Hengyang Medical School, University of South China, Hengyang 421000, Hunan Province, China
[3]Fujian Provincial Key Laboratory of Ophthalmology and Visual Science, Fujian Engineering and Research Center of Eye Regenerative Medicine, Xiamen 3611002, Fujian Province, China
[4]Department of Traditional Chinese Medicine, School of Medicine, Xiamen University, Xiamen 361100, Fujian Province, China
[5]Department of Ophthalmology, the First Affiliated Hospital of University of South China, Hengyang 421001, Hunan Province, China
Co-first authors: Yong Li and Ya-Qiong Yang
Correspondence to: Zu-Guo Liu. Key Laboratory of Ophthalmology, University of South China, Hengyang 421000, Hunan Province, China. zuguoliu@xmu.edu.cn
Received: 2024-01-18 Accepted: 2024-07-26

Abstract

● **AIM:** To establish a stable, short-time, low-cost and reliable murine model of meibomian gland dysfunction (MGD).

● **METHODS:** A filter paper sheet soaked in 1.0 mol/L sodium hydroxide (NaOH) solution was used to touch the eyelid margin of C57BL/6J mice for 10s to establish the model. The other eye was left untreated as a control group. Eyelid margin morphological changes and the meibomian glands (MGs) were observed by slit lamp microscopy on days 5 and 10 post-burn. Hematoxylin-eosin (HE) staining and Oil red O staining were adopted in detecting the changes in MGs morphology and lipid deposition. Real-time polymerase chain reaction, Western blot, immunofluorescence staining and immunohistochemical staining were used to detect interleukin (IL)-6, IL-1β, IL-18, tumor necroses factor (TNF)-α, interferon (IFN)-γ, nicotinamide adenine dinucleotide phosphate (NADPH) oxidase 4 (NOX4), 3-nitroturosine (3-NT), 4-hydroxynonenal (4-HNE) and cytokeratin 10 (K10) expression changes in MGs.

● **RESULTS:** MGs showed plugging of orifice, glandular deficiency, abnormal acinar morphology, ductal dilatation, and lipid deposition after alkali burn. The expressions of IL-6, IL-18, IL-1β, IFN-γ, and TNF-α indicators of inflammation and oxidative stress in MGs tissues were significantly increased. Abnormal keratinization increased in the MG duct.

● **CONCLUSION:** A murine model of MGD is established by alkali burn of the eyelid margin that matches the clinical presentation of MGD providing a stable, short-time, low-cost, and reliable MGD model. The new method suggests efficient avenues for future research.

● **KEYWORDS:** alkali burn; meibomian gland dysfunction; animal model; oxidative stress

DOI:10.18240/ijo.2024.12.02

Citation: Li Y, Yang YQ, Lin Y, Yan K, Lyu YF, Zhang ZQ, Huang CH, Hu JY, Liu ZG. Alkali burn injury model of meibomian gland dysfunction in mice. *Int J Ophthalmol* 2024;17(12):2158-2166

INTRODUCTION

Meibomian glands (MGs) play a critical role in the eyes. It is embedded in the eyelids and can produce meibum, a lipid secretion. When blinking eyes, the meibum is secreted and evenly distributed on the ocular surface[1]. Meibomian gland dysfunction (MGD) will affect the tear film stability and eventually disrupt ocular surface homeostasis, causing epithelial damage and even clinical symptoms like dryness, discomfort and ocular pain[2-3].

MGD is a chronic pervasive disorder of the MGs characterized by altered glandular secretion or stenosis of the terminal ducts. Therefore, eye irritation and symptoms of the ocular surface disease can result from the altered tear film[4]. As a result of MGD, tear film instability and inflammation of the ocular surface as well as symptoms of ocular surface irritation occur, making MGD one of the greatest important causative factors of dry eye and severely reducing the life quality of patients with dry eyes[5]. Many intrinsic and extrinsic risk factors can lead to MGD. Several pathological mechanisms are involved, including lipid deficiencies, inflammation, microbial factors,

and aging. Keratinization of the meibomian ducts, MGs inflammation, Hyper-evaporation, microbial proliferation, and toxic cytokines cause MGD and corneal injury. MGD is one of the commonest ophthalmic disorders worldwide[6]. Globally, the prevalence of MGD differs by region and age, ranging from 3.5% to 70%, with the highest prevalence of 49.2%–69.3% in the elderly[7-8]. The number of MGD patients is increasing yearly, but currently, there is no specific drug for MGD, which leads to an increased focus on further investigating MGD as well as an increased demand for a more reliable MGD animal model. However, the current MGD animal models still have a lot of controversies.

Alkali burn is one of the common injuries in life. Solutions that can cause alkali burn include sodium hydroxide (NaOH) solution, KOH solution, and high-concentration Na_2CO_3 solution. The body will suffer from alkali burn after the inflammatory reaction, regeneration of tissue structure in changes in glandular structure skin aging, *etc*[9-10]. Alkali burn is also a common experimental technique in animal experiments. It is generally used in constructing dry eye animal model and neovascular model[11-13]. Alkali burn is low-cost, simple, controllable, and can be induced in animals with different degrees of injury according to experimental needs. Thus, the animal models of alkali burn are more compatible with clinical cases and therefore more reflective of objective clinical changes[14-16].

Many clinical investigations have found that the normal physiological structure and function of the MGs are altered in patients with alkali burns and that the degree of MGD increases as the alkali burn worsens[17-18]. Currently, the most commonly used experiment animals in MGD research are rat and rabbit[19-24]. However, there are no reports on the use of alkali burn to induce MGD in mice. It is of great importance to find a reliable MGD animal model in mouse, because compared to rats and rabbits, mice offer more antibodies and are cheaper to use as experimental animals.

In this study, alkali burn was further used to induce MGD in mice. The morphological and structural changes of the MGs as well as the signs of inflammation associated with MGD were monitored to validate the reliability of the alkali burn induced MGD mouse model.

MATERIALS AND METHODS

Ethical Approval According to the Association for Research in Vision in Ophthalmology (ARVO) Statement for the Use of Animals in Ophthalmic and Vision Research, all studies were approved by the Animal Ethical Committee of Xiamen University.

Materials Anti-tumor necroses factor (TNF)-α (ab66579, abcam, UK), anti-cytokeratin 10 (K10, ab76318, abcam, UK), anti-nicotinamide adenine dinucleotide phosphate (NADPH) oxidase 4 (NOX4, ab133303, abcam, UK), anti-4-hydroxynonenal (4-HNE, ab46545, abcam, UK), the mouse anti-3-nitroturosine (3-NT, ab61392, abcam, UK) were from Abcam (Cambridge, UK). Anti-NOD-like receptor thermal protein domain associated protein 3 (NLRP3; 19771-1-AP, Proteintech, USA) was from Proteintech (Rosemont, USA). The Alexa Fluor 488-conjugated immunoglobulin G (IgG; A21206, Invitrogen, USA) was from Invitrogen (Eugene, OR, USA). Anti-β-actin antibody (AC026, ABclonal, China) was from ABclonal (Wuhan, China). Amounts of 6-diamidino-2-phenylindole (DAPI; H-1200, Vector, USA) and mounting medium (H-5000, Vector, USA) were provided by Vector (Burlingame, USA).

Animals In this study, male C57BL/6J mice between 12 and 15wk were purchased from Beijing Vital River Laboratory Animal Center (Beijing, China. XMULAC20200169 2020-12-18). We kept the animals in a pathogen-free environment between 25°C±1°C with 50% relative humidity and 12h cycles of light and dark (from 8 *a.m.* to 8 *p.m.*).

Animal Examination After the animals were procured, fed in the animal housing room for 1wk and were stabilized, an ophthalmologist examined the lid margins and corneas through a slit-lamp microscope (Kanghua Science & Technology Co. Ltd., Chongqing, China). The conjunctiva sac was then injected with a solution of 1% sodium fluorescein (Jingmingxin Co, Ltd., Tianjin, China). A slit-lamp microscope equipped with a cobalt blue filter film was used to observe and record the corneal epithelial fluorescein staining 15s later. According to the previously reported criteria, the corneal injury was graded[25]. Mice could not be enrolled in the experiment if they had positive sodium fluorescein staining and damaged lid margins. Six to eight mice per group were guaranteed.

Methods We divided 24 mice into model group (left eye) and control group (right eye). A filter paper sheet (2 mm diameter) soaked in 1.0 mol/L NaOH solution was used to touch the right central margin of mice for 10s, and immediately was irrigated with 5 mL physiological saline (0.9% NaCl) to establish the model (Figure 1), and the other eye was left untreated as a control group. Then the MG was irrigated with 5 mL physiological saline (0.9% NaCl).

Experimental Procedure Fluorescein staining was performed during the experiment in both groups (on days 0, 5, and 10). In the tenth day of the experiment, the MG tissue from all mice was carefully dissected and harvested for real-time polymerase chain reaction (PCR) analysis, Western blot, HE staining, Oil Red O staining, immunofluorescence staining, and immunohistochemistry following the methods described below.

Meibomian Glands Margin and Meibomian Glands Photography One person holds the mouse on the edge of

Figure 1 Eyelid margin of C57BL/6J mice was burned under a slit lamp with filter paper infiltrated with 1.0 mol/L NaOH solutions.

the microscope (Takagi Seiko Co. Ltd. Nagano, Japan) stage with the left hand and gently lifts the mouse's eyelid with the right hand so that the MGs margin is fully exposed and perpendicular to the light. The other person's right hand adjusts the angle of the light source to fully illuminate the MGs margin of the mouse and ensure that there is no reflection, while the left hand adjusts the focus, orientation, and angle of the microscope to take the picture. Mice eyelids were removed and photographed with a stereoscopic zoom microscope (M165-FC, Leica, Germany).

Fluorescein Sodium Staining Score In a slit-lamp examination, one microliter of 1% sodium fluorescein liquid was injected into the conjunctival sac. After three blinks and 15s, corneal epithelial damage was graded by cobalt blue filter. The cornea was divided into four quadrants and the total score is calculated: 0 points, no stain; 1 point, dotted with dye ≤30; 2 points, dotted with dye >30 but not diffuse; 3 points, dots are serious but not fused; and 4 points, the dye is patchy.

Hematoxylin-Eosin Staining After the eyelids were resected, fixation and dehydration of the eyelids tissue are performed according to the prescribed procedures. Dehydrated tissues were embedded in paraffin and sliced into 5 μm sections using a paraffin slicer (CM1950, Leica, Germany), and dried on a baking machine. Staining was first performed by dewaxing using xylene in two 15-minute cycles. Subsequently, dehydration was performed by a series of ethanol concentration decreases (100% ethanol concentration in two cycles, followed by 95%, 80%, and 70%). Hematoxylin staining was performed for 5min. The stained sections were then washed with distilled deionized water (DDW), fractionated in hydrochloric acid ethanol, and rinsed again with DDW. Finally, the stained sections were stained with eosin for 5min, dehydrated according to the experimental procedure, and sealed with H-5000. Stained sections were imaged under a microscope (Eclipse 50i, Nikon, Japan).

Oil Red O Staining Following the execution of the mice, the eyelids were removed and immediately put in 4% paraformaldehyde and placed in optimal cutting temperature compound. The frozen tissue blocks were cut into sections of 5 μm thickness using a frozen sectioning machine. It was then washed with 1× phosphate buffer solution (PBS) after being fixed for 5min. Initially soaked in 60% isopropanol for 10s, then stained with freshly prepared Oil Red O solution for 15min, followed by 3s of rinsing with 60% isopropanol. The sections were re-stained with hematoxylin for 5min. Tissue dehydration was performed according to the prescribed dehydration process, and finally, the sections were sealed with 90% glycerol. Stained sections were imaged under a microscope (Eclipse 50i, Nikon, Japan).

Immunofluorescence Staining The frozen sections were fixed for 15min with 4% paraformaldehyde. Following that, 2% bull serum albumin (BSA) was applied to tissue sections for 30min at 37°C to prevent nonspecific background staining and incubated with K10 (1:300) antibodies for 12h at 4°C. Sections were washed with PBS, then the sections were incubated with Alexa Fluor 488-conjugated IgG (1:300) for 60min at room temperature. Finally, the sample is stained with DAPI (H-1200). A microscope (DM2500, Leica, Germany) was then used to observe and photograph the sections.

Immunohistochemical Staining Paraffin sections were deparaffinized according to the protocol, fixed with 4% paraformaldehyde for 15min and washed with 1×PBS, and citrate buffer was used for antigen repairing at 100°C for 10min and again washed with 1×PBS. For 10min, 3% H_2O_2 was injected into methanol to inhibit endogenous peroxidase. Following this, tissue sections were blocked for 30min at room temperature with 2% BSA, followed by three washing cycles with 1×PBS. Incubating samples with NOX-4 (1:300), 4-HNE (1:300), and 3-NT (1:300) anti-bodies at 4°C for 12h. After 30min of incubation with biotin-labeled horse anti-mouse IgG serum, sections were treated for 30min with avidin-biotin-alkaline phosphatase complex, washed three times in 1×PBS and developed in 3,3'-diaminobenzidine (DAB) chromogen solution. Antibody-stained tissues were counterstained with hematoxylin for 2min and mounted. In the end, the slides were sealed with H-5000. Sections were then observed and photographed using the microscope (DM2500, Leica, Germany).

RNA Extraction and Quantitative Reverse Transcription Polymerase Chain Reaction The MGs of mice were removed and placed in Eppendorf (EP) tubes with 1 mL Trizol (15596018, Invitrogen, USA), and RNA from the tissue was extracted using the kit method and reverse transcribed into complementary deoxyribonucleic acid according to the instructions. A real-time fluorescent quantitative polymerase chain reaction (qPCR) instrument (12015137001, Roch, Switzerland) was used for processing, using the following thermal profile: 10min at 95°C, 10s at 90°C, 30s of annealing and extension at 60°C, and 40 cycles of annealing and

extension. A comparative cycle threshold (CT) method was used to analyze qPCR results, and an endogenous reference gene was adopted to calculate the relative expression of each target gene for normalization and calibration with the normal group. The primers of qRT-PCR used are summarized in Table 1.

Western Blot Analysis After mice were executed in each group, the MGs were removed in EP tubes with 0.1 mL RIPA and 1 μL protease and phosphatase inhibitors, MGs were ground to collect proteins, after SDS-PAGE electrophoresis and polyvinylidene fluoride (PVDF) membrane transfer, and blocked with 2% BSA for 1h; TNF-α (1:1000); NLRP3 (1:1000) and β-actin (1:10 000) was added separately for 12h in 4℃, 1×Tris buffered saline with tween (TBST) rinsed 3 times each time for 5–10min, and add goat anti-rabbit IgG antibody (1:500) and incubate for 1h, 1×TBST rinsed 3 times each time for 5–10min, The secondary antibodies were incubated for 2h with enhanced chemiluminescence reagent (P10300, NCM Biotech, China) in a transilluminator (ChemiDoc XRS System, Bio-Rad, USA).

Statistical Analysis The data were manipulated using GraphPad Prism 8.0 software (GraphPad Software Inc, SanDiego, CA, USA). One-way ANOVA was conducted to analyze differences in corneal fluorescein staining scores, The Mann-Whitney test was used to compare the differences in relative mRNA rates. A significance level of $P<0.05$ was considered statistically significant.

Table 1 Primers used in the study

Gene name	Sequence (5′-3′)
IL-1β-F	GCACTACAGGCTCCGAGATGAA
IL-1β-R	GTCGTTGCTTGGTTCTCCTTGT
INF-γ-F	CTTCAGCAACAGCAAGGCGAAA
INF-γ-R	CCGAATCAGCAGCGACTCCT
IL-6-F	CTTGGGACTGATGCTGGTGACA
IL-6-R	GCCTCCGACTTGTGAAGTGGTA
TNF-α-F	ACAGCAAGGGACTAGCCAGGAG
TNF-α-R	AGTGCCTCTTCTGCCAGTTCCA
K10-F	CTGGCGATGTGAACGTGGAA
K10-R	GTCCCTGAACAGTGCGTCTC
Actin-F	AGATCAAGATCATTGCTCCTCCT
Actin-R	ACGCAGCTCAGTAACAGTCC

IFN: Interferon; TNF: Tumor necroses factor; IL: Interleukin; K10: Cytokeratin 10.

RESULTS

Alkali Burn Leads to the Damage of Mice Eyelid Margin and Corneas The clinical symptoms of MGD are diverse and complex, including changes in eyelid morphology, altered secretions, and glands atrophy or dropout. A slit lamp is used to determine the morphological changes of mice eyelid margins, including meibomian orifice plugging, hyperemia, and telangiectasias. The eyelid of mice in the control group was smooth and flat, without eyelid margin thickening and MG orifices secretions blocked. As of the 5th day after alkali burn, MGs margins were uneven, blepharons showed hyperemia, part of the eyelid tissues showed edema, and partial MGs openings were blocked. The condition on the tenth day was similar to that of the fifth day, the MGs margin was uneven, the blepharoedema was subsided and partial MG openings were blocked by hoary secretions with neovascularization in the palpebral margin.

MGs is a key component of the tear film and assist maintain ocular surface microenvironment homeostasis. When these MGs are atrophic, absent or non-functional, the ocular surface will also suffer secondary damage. In our results, the ocular surface photography showed that there no white spots and clouds in the cornea of the control group and the alkali burn group in day 0, indicating that the alkali burn did not damage the corneal. We used corneal fluorescein staining to find out whether the corneal epithelium is defective. The results showed that the corneal epithelium was glossy and clear in control group and without diffuse staining. However, the corneas in the experimental group showed diffuse patchy staining with fluorescein staining on days 5 and 10 (Figure 2). The results show that alkali burn model can cause obstruction of MGs, neovascularization and secondary corneal injury in mice.

Alkali Burn Causes Obstruction and Atrophy of the MGs and Dilation of the Ductules To observe the changes in the MGs, the glands were photographed 5 and 10d after the alkali burn. MGs of the control group were intact and arranged in an orderly manner. The MGs in the experimental group showed distortion and atrophy on the fifth day, and the glands dropout was observed on the tenth day. Overall, the alkali burn mice demonstrate more extensive MGs dropout than the control group (Figure 3A). According to H&E staining, the main duct dilatations in the experimental group were severe, and the walls of the gland ducts were thickened (Figure 3B). There was more oil-red staining in gland ducts of alkali-burned mice, suggesting the accumulation of lipids in the MGs and indicating abnormal lipid metabolism in MGs (Figure 3C). It is evidence that MGs obstruction occurs in the alkali burn model, accompanied by MGs morphology and function alterations.

Oxidative Stress and Inflammatory Signaling Pathways Activated After Alkali Burn In alkali burn model, lipid oxidation may contribute to MGs inflammation. It is well known that oxidative processes promote inflammation in a lot of diseases and activate inflammatory cytokines to promote inflammation. 3-NT, NOX4, and 4-HNE are three important markers of oxidative stress. The 4-HNE is the most popular marker of lipid peroxidation, almost all 4-HNE comes from phospholipid-bound arachidonic acid.

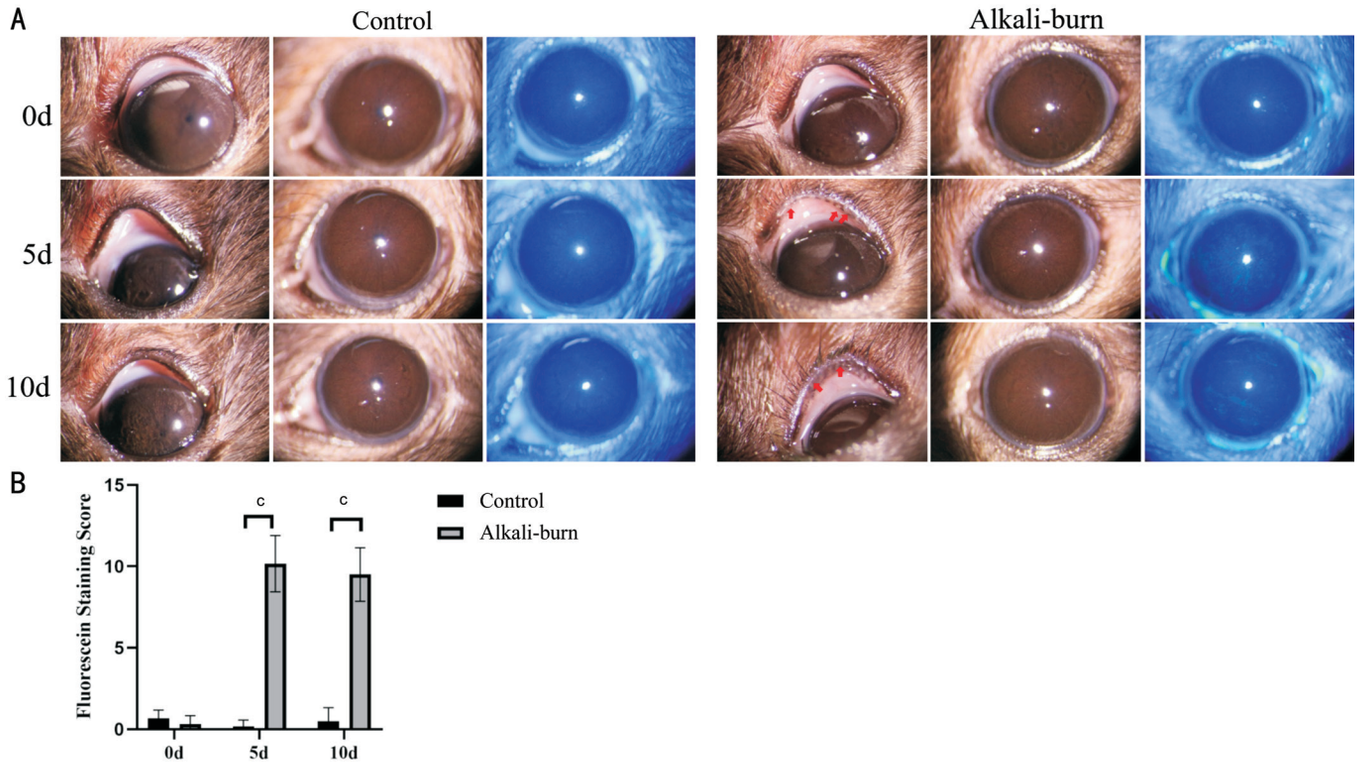

Figure 2 MGs and ocular surface of mice after alkali burn A: Morphological changes of mice eyelid margin and corneal fluorescein sodium staining on days 5 and 10 after alkali burn; B: The corneal fluorescein staining scores of each group of mice. Data are mean±SD, *n*=6. *P* values were calculated using two-tailed unpaired *t*-tests. $^{c}P<0.001$. SD: Standard deviation; MG: Meibomian gland.

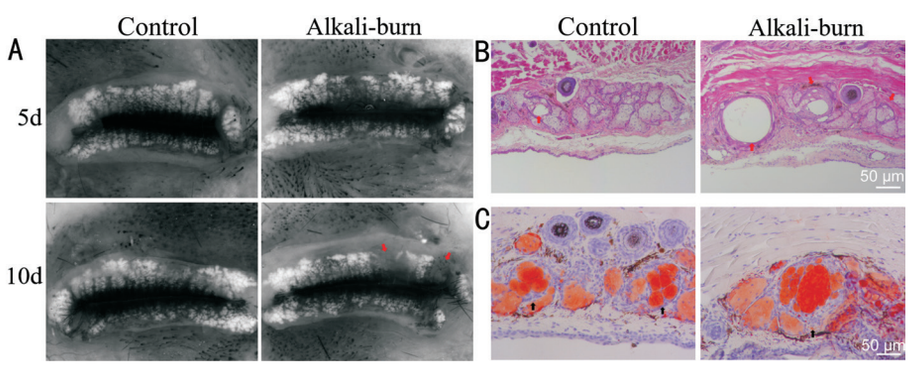

Figure 3 Histological changes of MGs in mice after alkali burn A: Changes of the MGs at 5 and 10d after alkali burn. Red arrows show the atrophy and drop out of the MGs. B: H&E staining of the MGs. Red arrows show the gland ducts of the MGs. C: Oil red staining of the MGs. Black arrows show the ducts of the MGs. H&E: Hematoxylin-eosin staining; MG: Meibomian gland.

A pathophysiological process, inflammation occurs when tissue is damaged or microbial invasion occurs. Multiple pro-inflammatory cytokines including TNF-α, interleukin (IL)-6, and IL-1β are activated in the injury response. Observations of immunohistochemistry showed that the expression of 3-NT, NOX4, and 4-HNE increased after alkali burn (Figure 4A) compared with the normal mice. We further explored the changes in inflammatory signaling pathways and inflammatory factors after alkali burn. Western blot was adopted to detect the expression level of TNF-α and NLRP3 in MGs. The expression level of TNF-α and NLRP3 was obviously increased in the alkali burn model (Figure 4B). Meanwhile, by real-time PCR, we examined the mRNA expression levels of interferon (IFN)-γ, TNF-α, IL-6, IL-18, and IL-1β in MGs were significantly increased compared to normal mice (Figure 4C).

Keratinization of the Meibomian Ducts in Alkali Burn Model Symptoms of obstructive MGD include degraded gland expansion and atrophy caused by hyperkeratinization of the ducts. An examination of the expression of K10 as a biomarker of epithelial keratinization was undertaken. The expression of K10 in the MGs after alkali burn was up-regulated by real-time PCR (Figure 5A). Further immunofluorescence staining showed that the expression of K10 in the MGs ducts of the alkali burn mice was higher than normal mice (Figure 5B). These results indicate that the alkali burn model can induce ductal hyperkeratinization, leading to obstructive MGD.

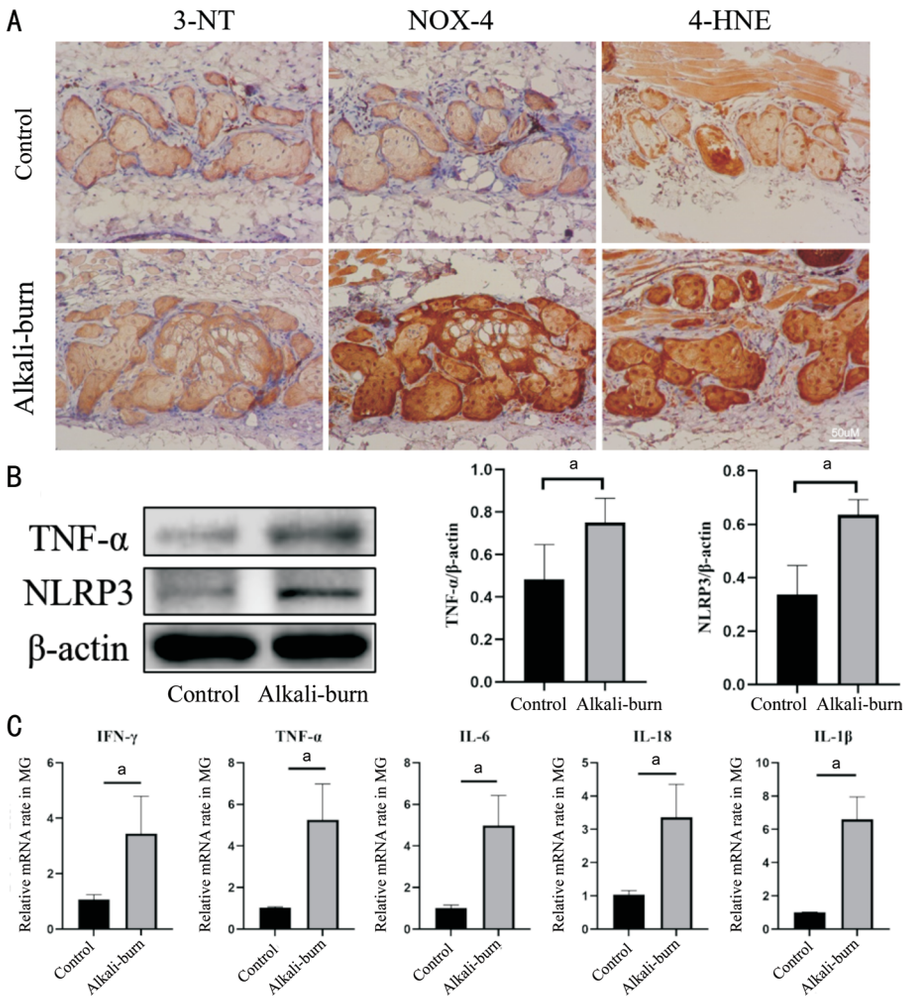

Figure 4 Expression of oxidative stress markers and inflammatory factors in MGs after alkali burn A: The immunohistochemical staining of 3-NT, NOX4, and 4-HNE in MGs. B: Western blot of the expression of TNF-α and NLRP3 in MGs; C: The mRNA expression level of IFN-γ, TNF-α, IL-6, IL-18, and IL-1β in MGs. Data are mean±SD. *n*=3. *P* values were calculated using two-tailed unpaired *t*-tests. [a]*P*<0.05. MG: Meibomian gland; NOX4: NADPH oxidase 4; 3-NT: 3-nitroturosine; 4-HNE: 4-Hydroxynonenal; IFN: Interferon; TNF: Tumor necroses factor; IL: Interleukin; NLRP3: NOD-like receptor thermal protein domain associated protein 3.

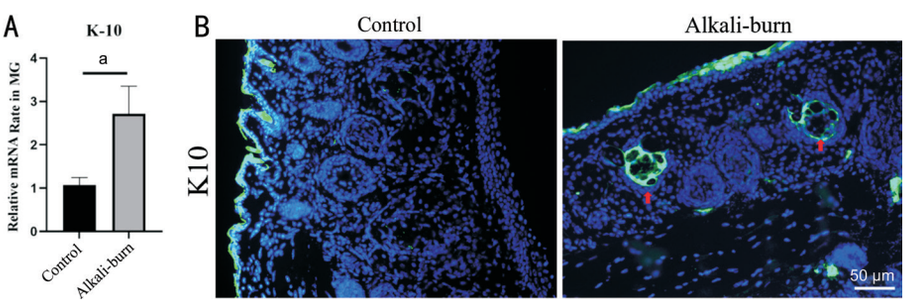

Figure 5 Keratinization of the meibomian gland duct in an alkali burn model A: mRNA expression of K10 in the MGs of normal mice and alkali burned mice. Data are mean±SD, *n*=3. *P* values were calculated using two-tailed unpaired *t*-tests. [a]*P*<0.05. B: Immunofluorescence analysis of K10 in the MGs of normal mice and alkali burned mice. Red arrows show the K10 expressing cells on the MGs ducts in the experimental group. MG: Meibomian gland; K10: Cytokeratin 10.

DISCUSSION

MGD is a chronic, diffuse abnormality of the MGs characterized by terminal duct obstruction and/or alteration in the quality/quantity of glandular secretions. MGD can cause changes in the tear film, symptoms of ocular irritation, significant inflammation even ocular surface disease. Among other things, tear film changes can seriously affect the ocular surface microenvironment homeostasis. The tear film is structured into the lipid layer, the aqueous layer and the mucin layer, of which the presence of the lipid layer is critical and functions as an aqueous barrier to prevent tear evaporation. The lipid layer of tear film is mainly secreted by MGs. Recent epidemiological

surveys have shown that the global prevalence of MGD is increasing year by year, which has become a human health concern[5-7].

As the researches focusing on MGD gradually increases, there is emerging evidence showing that the immunopathogenesis of MGD is complicated involving lipid composition changes, gland obstruction, loss of PPAR-γ expression, oxidative stress, chronic inflammation, *etc*[26-28]. Researchers' first hurdle was the lack of a suitable MGD animal model. From the 1980s onwards, Jester *et al*[29] found that injection of epinephrine into the rabbit eyelid can cause keratinization of the MGs catheter and induce MGD. With the further study of MGD, the pathogenesis of MGD was found to be extremely complex[30]. There is more than one cause of MGD, so animal models of MGD are time-consuming to construct, taking approximately six months accompanied by a low success rate. In the late 20th century, with rapid advances in gene technology, many MGD gene-deficient animal models appeared, including K5-GR mice, *Bark2*-null mice, *Eda*$^{-/-}$ mice, *Sod1*$^{-/-}$ mice, *ApoE*$^{-/-}$ mice, *etc*[31-35]. Genetic knockout can induce MGD in mice, and the success rate was higher. Undeniably, because of its significant animal cost and time, it is difficult to widely used. Besides, it requires feeding mice with a particular diet, rather than regular mouse chow. It is difficult to raise in large quantities.

In 2018, Dong *et al*[19] successfully developed a MGD model, with slim guidewires into the MGs orifices and destroy the MGs. However, this model is mostly used for rats not mice. The method is difficult to perform, and the major symptoms show late. These methods need higher requirements for researchers, which hinder researchers from using these animal models.

The MGs of C57BL/6J mice is similar to humans[24]. The C57BL/6J mice are the cheapest and the most widely used animals in research. Stable and reliable MGD model can be acquired with a simple and easy maneuver. Then this MGD model can be widely used in research. In this study, we burned the MGs marge with filter paper soaked with 1 mol/L NaOH solution for 10s. The wound surface was not too large and corneal injury was prevented by using an accurate location.

In present study, we used the experimental method of alkali burn to induce MGD of mice for the first time, which has been widely used in dry eye and neovascularization studies in other animals. Alkali burn has been previously reported to cause tissue damage with structural change and inflammatory storm generation[36-39]. As we know, secondary ocular surface injury is a common pathological phenomenon and clinical manifestation of MGD. The MGs-derived lipid layer keeps water from evaporating from the ocular surface. According to studies, patients with obstructive MGD had decreased tear evaporation rates, MGs dropout, poorly secreted meibum, and signs of inflammation. It was found that tear evaporation increased with MGD severity. In addition, the abnormal quality and quantity of meibum will bring about decreased tear lipid layers, hyperosmolar tears, and mechanical friction at the ocular surface, all of these can bring about ocular surface damage. Sodium fluorescein staining score was higher in patients with MGD than those without MGD[28]. In our results, alkali burn which induces positive fluorescein corneal staining in mice can result in secondary ocular surface injury. We also observed that alkali burn can induce obstruction of the MGs, dilated ductules, atrophy of glands, glands dropout, keratinization of ducts, hyperemia of the eyelid margin, epithelial defects in mice cornea and increased expression of inflammatory factors. The cornea is transparent without scar formation during our observation. Based on this, it can be concluded that the obtained model is compliant with the clinical requirements of MGD.

The etiology of MGD is tangled, it is determined by the integration of many factors. The dominant belief is that chronic inflammation is central to MGD, and hyperkeratinization, atrophy and imbalance in the oxidative stress system are important components of MGD[4,31,40-41]. Studies pointed out that the key link in the occurrence and development of MGD was chronic inflammatory reaction[19,42-43]. NLRP3 plays an essential role in inflammatory responses[44]. Several studies have demonstrated abnormalities in inflammation associated with dry eye. Animal models with dry eyes exhibit higher levels of inflammatory factors expression. People with dry eyes show elevated levels of various inflammatory markers, including cytokines, chemokines, and prostaglandins[45]. Therefore, we investigated whether the inflammation signaling pathway and inflammatory factors are activated in the alkali burn model. The results showed that the inflammation signaling pathway was activated and IL-18, IL-6, IFN-γ, IL-1β, and TNF-α inflammatory factors were highly expressed in MGs of the alkali burn model, further confirming the inflammatory environment of the MGs.

Hyperkeratinization is the primary cause of obstructive MGD, which results in gland dilatation and atrophy. In alkali burns model MGs, hematoxylin-eosin staining showed dilation and immunofluorescence analysis showed upregulated K10 expression. These results indicated that the MGs of alkali burn model mice undergoing hyperkeratosis induced MGD and glands dilatation or atrophy. An accumulation of lipids in the glands may lead to vicious cycle of pathological changes. We also observed atrophy and drop out of the lower MG without alkali burn operation. This may be related to the mice being the age and the lower MG structure[6].

Lipid peroxidation-induced oxidative stress is a keymechanisms contributing to MGD[31,34,40,46]. The hyperkeratinization of the

MGs duct could obstruct and exaggerate lipid accumulation in acinar cells, thereby inducing reactive oxygen species (ROS). Oxidative stress can raise the production of ROS, which induces the expression of inflammatory cytokines[47]. Therefore, in the present study, results showed highly expression of NOX-4, 3-NT, and 4-HNE in MG tissues and activated inflammation signaling pathway as well as the expression of inflammatory cytokines, which is consistent with MGD patients.

In brief, we created an MGD mice model by alkali burn in the eyelid margin that resembled the clinical presentation of MGD, furnishing a stable, short-time, low-cost and reliable MGD model. The new method suggested efficient avenues for future research.

ACKNOWLEDGEMENTS

Foundations: Supported by the National Natural Science Foundation of China (No.82271054; No.U20A20363).

Conflicts of Interest: Li Y, None; **Yang YQ,** None; **Lin Y,** None; **Yan K,** None; **Lyu YF,** None; **Zhang ZQ,** None; **Huang CH,** None; **Hu JY,** None; **Liu ZG,** None.

REFERENCES

1 Green-Church KB, Butovich I, Willcox M, Borchman D, Paulsen F, Barabino S, Glasgow BJ. The international workshop on meibomian gland dysfunction: report of the subcommittee on tear film lipids and lipid-protein interactions in health and disease. *Invest Ophthalmol Vis Sci* 2011;52(4):1979-1993.

2 Watanabe K, Yoshida M, Okumura T, Sassa T, Kihara A, Uchiyama A. Improvement of evaporative dry eye with meibomian gland dysfunction in model mice by treatment with ophthalmic solution containing mineral oil. *Transl Vis Sci Technol* 2021;10(4):21.

3 Tao JP, Shen JF, Aakalu VK, Foster JA, Freitag SK, McCulley TJ, Vagefi MR, Kim SJ, Wladis EJ. Thermal pulsation in the management of meibomian gland dysfunction and dry eye: a report by the American academy of ophthalmology. *Ophthalmology* 2023;130(12):1336-1341.

4 Kim WJ, Ahn YJ, Kim MH, Kim HS, Kim MS, Kim EC. Lipid layer thickness decrease due to meibomian gland dysfunction leads to tear film instability and reflex tear secretion. *Ann Med* 2022;54(1):893-899.

5 McCann P, Abraham AG, Mukhopadhyay A, *et al*. Prevalence and incidence of dry eye and meibomian gland dysfunction in the United States: a systematic review and meta-analysis. *JAMA Ophthalmol* 2022;140(12):1181-1192.

6 Tian L, Guo YH, Wang SL, Li ZY, Wang NL, Jie Y. Efficacy of far infrared functional glasses in the treatment of meibomian gland dysfunction-related dry eye. *MedComm* 2024;5(4):e507.

7 Schaumberg DA, Nichols JJ, Papas EB, Tong L, Uchino M, Nichols KK. The international workshop on meibomian gland dysfunction: report of the subcommittee on the epidemiology of, and associated risk factors for, MGD. *Invest Ophthalmol Vis Sci* 2011;52(4):1994-2005.

8 Hassanzadeh S, Varmaghani M, Zarei-Ghanavati S, Heravian Shandiz J, Azimi Khorasani A. Global prevalence of meibomian gland dysfunction: a systematic review and meta-analysis. *Ocul Immunol Inflamm* 2021;29(1):66-75.

9 Huang YQ, Lin LX, Yang Y, Duan F, Yuan ME, Lou BS, Lin XF. Effect of tauroursodeoxycholic acid on inflammation after ocular alkali burn. *Int J Mol Sci* 2022;23(19):11717.

10 Walsh K, Hughes I, Dheansa B. Management of chemical burns. *Br J Hosp Med* 2022;83(3):1-12.

11 Chen MX, Chen XN, Li XQ, Wang JY, Wu J, Wang Q, Huang YF, Li ZJ, Wang LQ. Subconjunctival administration of mesenchymal stem cells alleviates ocular inflammation in a murine model of corneal alkali burn. *Stem Cells* 2023;41(6):592-602.

12 Hua X, Yuan XY, Li YH, Chen H, Yuan J, Tanumiharjo S, Bian F, Su LS, Hong YH, Liu YZ, Chi W. Desiccating stress worsens alkali burn injury by magnifying caspase-8-induced imbalance of NLRP3 and NLRP6. *J Allergy Clin Immunol* 2017;140(4):1172-1176.e3.

13 Yu JF, Shen Y, Luo JW, Jin J, Li PF, Feng PD, Guan HJ. Upadacitinib inhibits corneal inflammation and neovascularization by suppressing M1 macrophage infiltration in the corneal alkali burn model. *Int Immunopharmacol* 2023;116:109680.

14 Chung JH. Healing of rabbit corneal alkali wounds *in vitro*. *Cornea* 1990;9(1):36-40.

15 Giacomini C, Ferrari G, Bignami F, Rama P. Alkali burn versus suture-induced corneal neovascularization in C57BL/6 mice: an overview of two common animal models of corneal neovascularization. *Exp Eye Res* 2014;121:1-4.

16 Prasad D, Salman M, Reddy AA, *et al*. A review of rabbit models of meibomian gland dysfunction and scope for translational research. *Indian J Ophthalmol* 2023;71(4):1227-1236.

17 Clare G, Bunce C, Tuft S. Amniotic membrane transplantation for acute ocular burns. *Cochrane Database Syst Rev* 2022;9(9):CD009379.

18 Swarup A, Ta CN, Wu AY. Molecular mechanisms and treatments for ocular symblephara. *Surv Ophthalmol* 2022;67(1):19-30.

19 Dong ZY, Ying M, Zheng J, Hu LJ, Xie JY, Ma Y. Evaluation of a rat meibomian gland dysfunction model induced by closure of meibomian gland orifices. *Int J Ophthalmol* 2018;11(7):1077-1083.

20 Ibrahim MAA, Elwan WM. Role of topical dehydroepiandrosterone in ameliorating isotretinoin-induced Meibomian gland dysfunction in adult male albino rat. *Anat Anz* 2017;211:78-87.

21 Miyake H, Oda T, Katsuta O, Seno M, Nakamura M. A novel model of meibomian gland dysfunction induced with complete Freund's adjuvant in rabbits. *Vision* 2017;1(1):10.

22 Shi L, Li LJ, Sun XY, Chen YY, Luo D, He LP, Ji HJ, Gao WP, Shen HX. Er-Dong-Xiao-Ke decoction regulates lipid metabolism *via* PPARG-mediated UCP2/AMPK signaling to alleviate diabetic meibomian gland dysfunction. *J Ethnopharmacol* 2024;333:118484.

23 Bu JH, Wu Y, Li KC, Zhang MJ, Zhang RR, Sun L, Guo YL, He H, Li SY, Liu ZG, Li W. Transitory alkali exposure on meibomian gland orifices induces meibomian gland dysfunction. *Ocul Surf* 2023;29:406-415.

24 Sun M, Moreno IY, Dang M, Coulson-Thomas VJ. Meibomian gland

dysfunction: what have animal models taught us? *Int J Mol Sci* 2020;21(22):E8822.

25 Lin ZR, Liu XC, Zhou T, Wang YH, Bai L, He H, Liu ZG. A mouse dry eye model induced by topical administration of benzalkonium chloride. *Mol Vis* 2011;17:257-264.

26 Chhadva P, Goldhardt R, Galor A. Meibomian gland disease: the role of gland dysfunction in dry eye disease. *Ophthalmology* 2017;124(11S):S20-S26.

27 Jester JV, Brown DJ. Wakayama symposium: peroxisome proliferator-activated receptor-gamma (PPARγ) and meibomian gland dysfunction. *Ocul Surf* 2012;10(4):224-229.

28 Sabeti S, Kheirkhah A, Yin J, Dana R. Management of meibomian gland dysfunction: a review. *Surv Ophthalmol* 2020;65(2):205-217.

29 Jester JV, Rife L, Nii D, Luttrull JK, Wilson L, Smith RE. *In vivo* biomicroscopy and photography of meibomian glands in a rabbit model of meibomian gland dysfunction. *Invest Ophthalmol Vis Sci* 1982;22(5):660-667.

30 Kojima T, Dogru M, Kawashima M, Nakamura S, Tsubota K. Advances in the diagnosis and treatment of dry eye. *Prog Retin Eye Res* 2020:100842.

31 Bu J, Wu Y, Cai X, *et al*. Hyperlipidemia induces meibomian gland dysfunction. *Ocul Surf* 2019;17(4):777-786.

32 Cascallana JL, Bravo A, Donet E, Leis H, Lara MF, Paramio JM, Jorcano JL, Pérez P. Ectoderm-targeted overexpression of the glucocorticoid receptor induces hypohidrotic ectodermal dysplasia. *Endocrinology* 2005;146(6):2629-2638.

33 Cui CY, Smith JA, Schlessinger D, Chan CC. X-linked anhidrotic ectodermal dysplasia disruption yields a mouse model for ocular surface disease and resultant blindness. *Am J Pathol* 2005;167(1):89-95.

34 Ibrahim OM, Dogru M, Matsumoto Y, Igarashi A, Kojima T, Wakamatsu TH, Inaba T, Shimizu T, Shimazaki J, Tsubota K. Oxidative stress induced age dependent meibomian gland dysfunction in Cu, Zn-superoxide dismutase-1 (Sod1) knockout mice. *PLoS One* 2014;9(7):e99328.

35 Tsau C, Ito M, Gromova A, Hoffman MP, Meech R, Makarenkova HP. Barx2 and Fgf10 regulate ocular glands branching morphogenesis by controlling extracellular matrix remodeling. *Development* 2011;138(15):3307-3317.

36 Kasamatsu M, ARIMA T, Ikebukuro T, Nakano Y, Tobita Y, Uchiyama M, Shimizu A, Takahashi H. Prophylactic instillation of hydrogen-rich water decreases corneal inflammation and promotes wound healing by activating antioxidant activity in a rat alkali burn model. *Int J Mol Sci* 2022;23(17):9774.

37 Li QY, Hua X, Li LP, Zhou XY, Tian Y, Deng Y, Zhang M, Yuan XY, Chi W. AIP1 suppresses neovascularization by inhibiting the NOX4-induced NLRP3/NLRP6 imbalance in a murine corneal alkali burn model. *Cell Commun Signal* 2022;20(1):59.

38 Meng J, Lin B, Huang S, Li Y, Wu P, Zhang F, Ke Y, Hei X, Huang D. Melatonin exerts anti-angiogenic and anti-inflammatory effects in alkali-burned corneas. *Ann Transl Med* 2022;10(8):432.

39 Wang K, Jiang L, Zhong YY, Zhang Y, Yin QC, Li S, Zhang XB, Han HJ, Yao K. Ferrostatin-1-loaded liposome for treatment of corneal alkali burn *via* targeting ferroptosis. *Bioeng Transl Med* 2022;7(2):e10276.

40 Tapia G, Valenzuela R, Espinosa A, Romanque P, Dossi C, Gonzalez-Mañán D, Videla LA, D'Espessailles A. N-3 long-chain PUFA supplementation prevents high fat diet induced mouse liver steatosis and inflammation in relation to PPAR-α upregulation and NF-κB DNA binding abrogation. *Mol Nutr Food Res* 2014;58(6):1333-1341.

41 Jester JV, Parfitt GJ, Brown DJ. Meibomian gland dysfunction: hyperkeratinization or atrophy? *BMC Ophthalmol* 2015;15(Suppl 1):156.

42 Qazi Y, Kheirkhah A, Blackie C, Cruzat A, Trinidad M, Williams C, Korb DR, Hamrah P. *In vivo* detection of clinically non-apparent ocular surface inflammation in patients with meibomian gland dysfunction-associated refractory dry eye symptoms: a pilot study. *Eye(Lond)* 2015;29(8):1099-1110.

43 Perez VL, Mousa HM, Soifer M, Beatty C, Sarantopoulos S, Saban DR, Levy RB. Meibomian gland dysfunction: a route of ocular graft-versus-host disease progression that drives a vicious cycle of ocular surface inflammatory damage. *Am J Ophthalmol* 2023;247:42-60.

44 Kracht M, Müller-Ladner U, Schmitz ML. Mutual regulation of metabolic processes and proinflammatory NF-κB signaling. *J Allergy Clin Immunol* 2020;146(4):694-705.

45 Nixon GF. Sphingolipids in inflammation: pathological implications and potential therapeutic targets. *Br J Pharmacol* 2009;158(4):982-993.

46 Seen S, Tong L. Dry eye disease and oxidative stress. *Acta Ophthalmol* 2018;96(4):e412-e420.

47 Wu H, Wang Y, Zhang YP, Xu F, Chen JP, Duan LL, Zhang TT, Wang J, Zhang FJ. Breaking the vicious loop between inflammation, oxidative stress and coagulation, a novel anti-thrombus insight of nattokinase by inhibiting LPS-induced inflammation and oxidative stress. *Redox Biol* 2020;32:101500.